Steel and Composite Structures, Vol. 4, No. 1 (2004) 49-75
DOI: http://dx.doi.org/10.12989/scs.2004.4.1.049

Distortional buckling formulae for cold-formed steel rack-section members

N. Silvestre† and D. Camotim‡

Department of Civil Engineering, IST, Technical University of Lisbon,
Av. Rovisco Pais, 1049-001 Lisboa, Portugal

(Received September 16, 2003, Accepted February 3, 2004)

Abstract. The paper derives, validates and illustrates the application of GBT-based formulae to estimate distortional critical lengths and bifurcation stress resultants in cold-formed steel rack-section columns, beams and beam-columns with arbitrarily inclined mid-stiffeners and four support conditions. After a brief review of the Generalised Beam Theory (GBT) basics, the main concepts and procedures employed to obtain the formulae are addressed. Then, the GBT-based estimates are compared with exact results and, when possible, also with values yielded by formulae due to Lau and Hancock, Hancock and Teng *et al*. A few remarks on novel aspects of the rack-section beam-column distortional buckling behaviour, unveiled by the GBT-based approach, are also included.

Key words: distortional buckling; distortional buckling formulae; generalised beam theory (GBT); rack-section members; flexural end support conditions; warping end support conditions.

1. Introduction

A distortional buckling mode was first reported by Van der Maas (1954), in the context of thin-walled hat-section columns. He described it as "a distinct kind of 'local' buckling mode configuration characterised by the occurrence of simultaneous web flexural deformations and lateral movements of the flanges and stiffeners". Nowadays, *distortional buckling* designates a specific type of bifurcation instability: the member axis remains undeformed and the in-plane cross-section deformations involve (i) moderate plate bending and (ii) *fold line motions*. The latter induce cross-section *distortion* and are the "trademark" of this buckling phenomenon. Figs. 1(a)-(b) show the geometry and distortional buckling mode (DM) shapes of rack-section[1] columns and beams.

Experimental analyses and numerical simulations performed in thin-walled members with single-wall webs clearly showed that (i) relevant flexural deformations appear only in the web and (ii) the compressed flange-stiffener assemblies remain practically undeformed - they just rotate about the web-flange longitudinal edge (see Fig. 1(b)). Based on this evidence, Lau & Hancock (1987) unveiled the similarity between (i) the thin-walled member distortional buckling behaviour and (ii) the flexural-torsional buckling behaviour of the (uniformly compressed) structural model depicted in Fig. 1(c_1)

†Research Assistant and Ph.D Candidate
‡Associate Professor
[1]Designation stemming from the frequent use of these cold-formed steel profiles in storage racks (Hancock 1985).

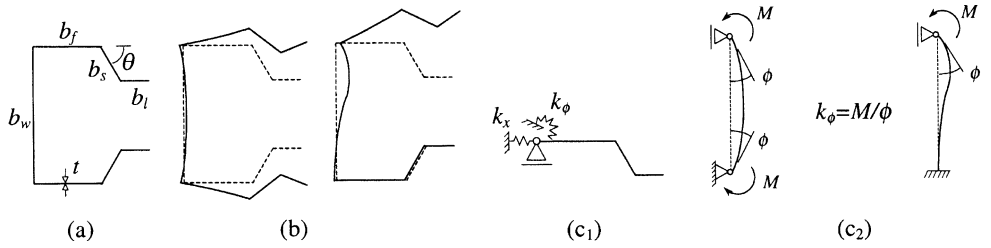

Fig. 1 Rack-section (a) geometry, (b) column and beam DM configurations; (c) Lau & Hancock's (c_1) model and (c_2) column and beam web deformed configurations

("flange-stiffener strut" elastically supported along the web-flange edge). Subsequently, (i) Lau & Hancock (1987), for C, Z and rack-section columns, (ii) Hancock (1997), for C and Z-section beams, and (iii) Bambach *et al.* (1998), for C and Z-section columns and beams with double-lip stiffeners, used this model to develop formulae to estimate distortional buckling stresses in columns and beams with pinned and free-to-warp end sections. Some of these formulae are now routinely employed and a few have already been included in the Australia/New Zealand cold-formed steel code (SAA 1996). Since Lau and Hancock's approach breaks down for members with very slender webs, Schafer (1997) and Davies & Jiang (1998) proposed slight modifications, both for columns and beams. Recently, Teng *et al.* (2003) extended the application of Lau & Hancock's model to C and rack-section beam-columns (bending in the plane of symmetry only).

Very recently, the authors used Generalized Beam Theory (GBT) (Schardt 1989, 1994a) to derive fully analytical distortional buckling formulae for C and Z-section cold-formed steel members (Silvestre & Camotim 2003)[2]. It seems fair to regard them as "superior" to the ones proposed by Lau & Hancock (1987), Hancock (1997), Schafer (1997) and Teng *et al.* (2003), in the sense that they (i) consistently yield equally or more accurate estimates and (ii) can be applied to a wider range of members (all other formulae apply only to members with pinned and free-to-warp end sections). However, symbolic manipulation limitations preclude using the derivation technique previously employed to obtain formulae for cross-sections with more than *five* walls, such as rack-sections (seven walls). In order to overcome this five-wall limitation, a slightly different technique was recently developed (Silvestre *et al.* 2002) and applied to rack-section columns and beams with pinned and free-to-warp or fixed and warping-prevented end sections. Since it requires the *numerical* solution of an auxiliary standard eigenvalue problem, it was termed as "quasi-analytical".

The objective of this work is to present the derivation, validate and illustrate the application of GBT-based distortional buckling formulae for cold-formed steel rack-section columns (uniform compression), beams (pure bending) and beam-columns (combination of both) with arbitrarily inclined mid-stiffeners (see Fig. 1(a)). Four support conditions are dealt with, namely members with (i) both end sections pinned and free-to-warp, (ii) both end sections fixed and warping-prevented, (iii) one end section fixed and warping-prevented and the other pinned and free-to-warp and (iv) one end section fixed and warping-prevented and the other "sliding" and warping-prevented. The formulae are still "quasi-analytical", *i.e.*, require the *numerical* solution of an auxiliary eigenvalue problem, which is *analytically defined* in terms of the member cross-section dimensions. In order to (i) assess the accuracy and validity and (ii) illustrate the application and capabilities of the proposed distortional buckling formulae, numerical

[2]Note that Schardt himself exploited the use of GBT to derive distortional buckling formulae (Schardt 1994b).

results are presented and discussed. The GBT-based estimates are compared with (i) exact results and, for pinned and free-to-warp members only, also with (ii) values yielded by the formulae due to Lau & Hancock (1987), Hancock (1997) and Teng *et al.* (2003). The paper also includes a few remarks on novel aspects of the distortional buckling behaviour of rack-section beam-columns, unveiled by the present GBT-based approach.

2. Brief GBT outline

The application of second order GBT (Schardt 1989, Davies *et al*. 1994, Silvestre & Camotim 2002a,b) leads to the system of equilibrium equations (one per deformation mode)

$$EC_{ij}\phi_{j,xxxx} - GD_{ij}\phi_{j,xx} + B_{ij}\phi_j + W_k X_{kij}\phi_{j,xx} = 0 \tag{1}$$

where (i) x is the axial coordinate, (ii) function $\phi_j(x)$ provides the longitudinal variation of the mode j amplitude, (iii) E and G are Young's and shear moduli and (iv) $(\cdot)_{,x} = d(\cdot)/dx$. In each equation, (i) the first three terms concern the member 1st order behaviour and (ii) the last one deals with the 2nd order effects (interaction between cross-section normal stresses and out-plane deformations). The tensor components C_{ij} (warping constant), D_{ij} (torsion constant), B_{ij} (transverse bending stiffness) and X_{kij} (geometric stiffness related to stress resultant W_k), related to modes i and j, are given by

$$C_{ij} = t\int_b u_i u_j ds \qquad D_{ij} = \frac{1}{3}t^3\int_b w_{i,s} w_{j,s} ds \qquad B_{ij} = K\int_b w_{i,ss} w_{j,ss} ds$$

$$K_{kij} = \frac{t}{C_{kk}}\int_b u_k (v_i v_j + w_i w_j) ds \qquad W_k = -EC_{ik}\phi_{k,xx} \tag{2}$$

where (i) t and K are the wall thickness and bending stiffness ($K = Et^3/12(1-\nu^2)$), (ii) s is the cross-section mid-line coordinate, (iii) $(\cdot)_{,s} = d(\cdot)/ds$ and (iv) u, v and w are warping, membrane and flexural displacements along x, s and z (see Fig. 2).

A GBT stability analysis comprises a *cross-section* and a *member* analysis: while the former identifies the cross-section deformation modes and evaluates the modal properties (C_{ij}, D_{ij}, B_{ij}, X_{kij}), the latter establishes and solves the member equilibrium equations and boundary conditions, on the basis of its cross-section geometry, material properties, length, support conditions and applied load.

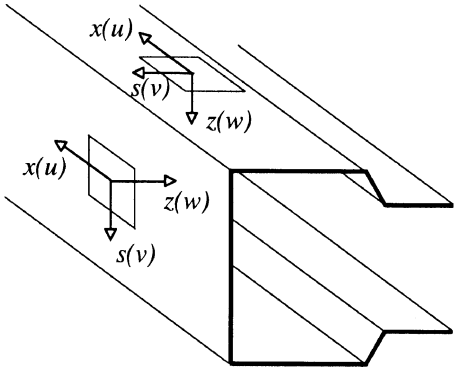

Fig. 2 Local coordinate system and displacement components

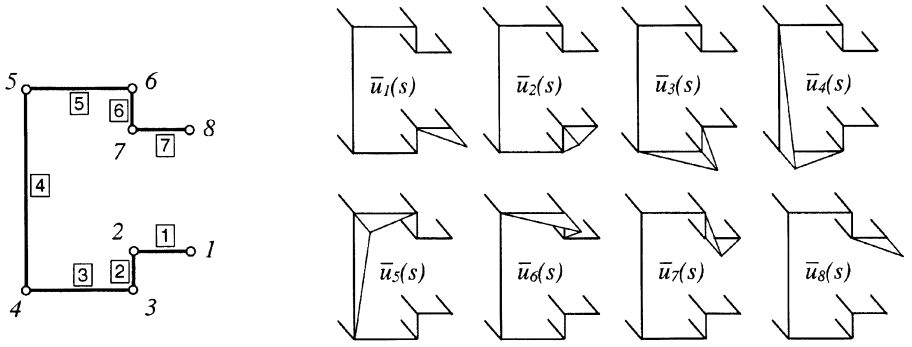

Fig. 3 Rack-section (a) discretisation and (b) elementary warping functions $\bar{u}_k(s)$ ($\theta = 90^o$)

2.1. Cross-section analysis

The performance of a GBT the *cross-section* analysis, for a cross-section with n walls and $n+1$ nodes ($n=7$ for the a rack-section - see Fig. 3(a)), involves the following operations:

(i) Obtain displacement functions $u(s)$, $v(s)$ and $w(s)$, by imposing unit warping displacements in each node ($\bar{u}_k = -1$, $k = 1...n+1$ – see Fig. 3(b)), which leads to the identification of $n+1$ "warping functions" $\bar{u}_k(s)$, varying linearly between consecutive nodes.

(ii) Using Vlasov's null shear strain assumption ($\gamma_{xs}^M = 0$) and the force method to obtain the cross-section deformed configurations due to the $\bar{u}_k(s)$ - constant $v_k(s)$, linear $u_k(s)$ and cubic $w_k(s)$. Compatibility between $v_k(s)$ and $w_k(s)$ is ensured.

(iii) Calculate matrices **C** and **B** (see Eqs. (2)), which are *fully populated* (*i.e.*, Eqs. (1) are *highly* coupled). Their components have no obvious physical meaning, even for trivial phenomena.

(iv) Diagonalise the above matrices, by solving the eigenvalue problem

$$(\boldsymbol{B} - \lambda_\alpha \boldsymbol{C})\boldsymbol{u}_\alpha = 0 \quad (\alpha = 1,..., n+1) \tag{3}$$

operation which comprises several stages and constitutes a key GBT feature (Schardt 1989, Silvestre & Camotim 2002a,b). One is led to $n+1$ eigenvectors of the form

$$\boldsymbol{u}_\alpha = \{u_1\ u_2\ ...\ ...\ u_n\ u_{n+1}\}^T \tag{4}$$

one per *deformation mode* (see Fig. 4(a)). The $\boldsymbol{u}_\alpha$ components are the axial (warping) displacement nodal values of mode α (see Fig. 4(b)).

(v) Calculate the axial (u_k) and transverse (v_k, w_k) displacement nodal values associated with each deformation mode.

Since rack-sections have *8* nodes, they exhibit *8 orthogonal* deformation modes: (i) the first four (1 - extension; 2 and 3 - major and minor axis bending; 4 - torsion) are rigid-body motions, for which $B_{kk} = 0$ ($w_{k,ss} = 0$ - see 2)), while (ii) the remaining four (modes 5 - 8), termed distortional modes, involve cross-section deformation with non-null transverse curvatures ($w_{k,ss} \neq 0$), *i.e.*, $B_{kk} \neq 0$.

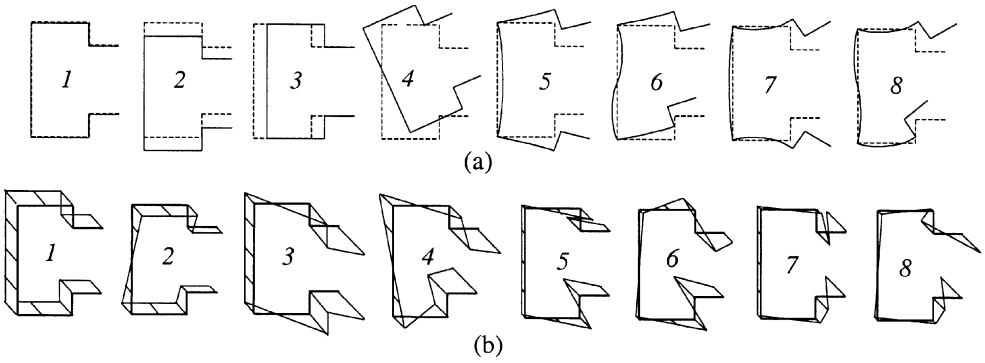

Fig. 4 GBT deformation modes: (a) in-plane configurations (b) warping displacements

2.2. Member (linear stability) analysis

After incorporating the (i) cross-section modal properties C_{ij}, B_{ij}, D_{ij}, X_{kij}, (ii) material constants E, ν, G, (iii) quantities related to the applied loads (W_k) and (iv) member length and support conditions into Eqs. (1), the n-dimension eigenvalue problem providing the member stability behaviour (expressed in terms of deformation mode amplitudes $\phi_j(x)$) is totally defined. A major advantage of the GBT approach is the possibility of performing "approximate (but accurate) stability analyses": one solves only the "subsystem" of Eqs. (1) corresponding to a few selected deformation modes. This unique feature is essential to derive the distortional buckling formulae.

3. Derivation of distortional buckling formulae

The observation of Fig. 4(a) shows that the rack-section distortional deformation modes can be divided into two groups: (i) modes 5 and 6, involving the distortion of the compressed three-wall flange-stiffener assemblies (rotation about the web-flange edge and plate bending only in the web) and (ii) modes 7 and 8, involving the distortion of only the compressed two-lip stiffeners (rotation about the flange-stiffener and plate bending in the web and compressed flanges). Since it has been recognised that, in general, the latter group plays a negligible role in the distortional buckling behaviour of rack-section members (Bambach *et al*. 1998[3]), this work addresses only DM combining deformation modes 5 and 6, from now on designated as follows: (i) mode 5 by S (web bends in *single* curvature) and (ii) mode 6 by D (web bends in *double* curvature).

Modes S and D are associated with (i) mechanical properties C_S, B_S, D_S and C_D, B_D, D_D and, depending on the applied load, also with (ii) one or more geometric stiffness properties X_S, X_D, X_S^{II}, X_D^{II}, X_{SD}^{I}. The amplitude functions $\phi_S(x)$ and $\phi_D(x)$ provide the cross-section displacement variation along the member length. If one is to derive fully analytical formulae, the above properties must be expressed in terms of the cross-section geometry (b_w, b_f, b_s, b_l, θ, t) and material constants (E, ν).

The derivation of the GBT-based distortional buckling formulae is presented in two stages: (i) deriving the formulae in terms of the distortional properties (this section) and (ii) determining analytical expressions to calculate these properties (next section). First, one must recognise that the DM shape of

[3]These authors designated this type of DM as "flange-lip DM" and stated that it is never likely to be critical.

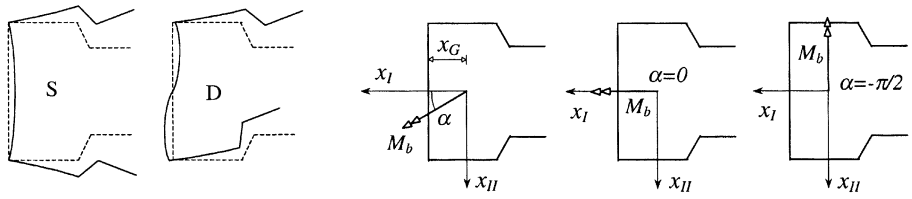

(a) (b)

Fig. 5 (a) GBT modes required to approximate an arbitrary beam-column DM shape (b) Bending about (b_1) an arbitrary neutral axis, (b_2) the *I-axis* and (b_2) the *II-axis*

any *beam-column* (bending about an *arbitrary* neutral axis) can always be closely approximated by a combination of modes S and D, shown in Fig. 5(a). Thus, even if the formulae are presented separately for *columns*, *beams* and *beam-columns*, the first two are to be regarded as special cases of the third one (note that the column DM shape involves only mode S - see Fig. 1(b)).

Because all GBT properties are evaluated w.r.t. the cross-section central principal axes, one starts by defining a consistent notation. Since, for the most common rack-section dimensions, the major (*I-axis*) and minor (*II-axis*) axes are parallel to the flanges and web, respectively, one adopts the following convention: *I-axis* and *II-axis* always stand for the *symmetry* and *non-symmetry* axes, regardless of the cross-section dimensions. Moreover, to avoid unnecessary repetitions, one denotes "members bending about the *I-axis* (*II-axis*)" by *I-axis (II-axis) members*. Moreover, x_G (see Fig. 5(b)) is the distance from the cross-section centroid G to the web.

Denoting the beam-column (i) bifurcation stress parameter by λ_b and (ii) compressive load and bending moment reference values by $\overline{P}$ and $\overline{M}$, bifurcation occurs when the applied stress resultants reach the values $P_b = \lambda_b \overline{P}$ and $M_b = \lambda_b \overline{M}$ (columns and beams are particular cases, for which $\overline{M}$=0 and $\overline{P}$=0). Then, the GBT equation subsystem for modes S and D reads (see Eqs. (1))

$$E \cdot \begin{bmatrix} C_S & 0 \\ 0 & C_D \end{bmatrix} \begin{Bmatrix} \phi_{S,xxxx} \\ \phi_{D,xxxx} \end{Bmatrix} - G \cdot \begin{bmatrix} C_S & 0 \\ 0 & C_D \end{bmatrix} \begin{Bmatrix} \phi_{S,xx} \\ \phi_{D,xx} \end{Bmatrix} + \begin{bmatrix} B_S & 0 \\ 0 & B_D \end{bmatrix} \begin{Bmatrix} \phi_S \\ \phi_D \end{Bmatrix} +$$
$$+\lambda_b \left(\overline{P} \begin{bmatrix} X_S & 0 \\ 0 & X_D \end{bmatrix} + \overline{M} \cos\alpha \begin{bmatrix} 0 & X^I_{SD} \\ X^I_{SD} & 0 \end{bmatrix} + \overline{M} \sin\alpha \begin{bmatrix} X^{II}_S & 0 \\ 0 & X^{II}_D \end{bmatrix} \right) \begin{Bmatrix} \phi_{S,xx} \\ \phi_{D,xx} \end{Bmatrix} = 0 \tag{5}$$

where the mode S and D properties, further addressed in section **4**., are evaluated by means of

$$C_S = t\int_b u_S^2 ds \qquad D_S = \frac{1}{3}t^3 \int_b w_{S,s}^2 ds \qquad B_S = K\int_b w_{S,ss}^2 ds$$
$$C_D = t\int_b u_D^2 ds \qquad D_D = \frac{1}{3}t^3 \int_b w_{D,s}^2 ds \qquad B_D = K\int_b w_{D,ss}^2 ds$$
$$X_S = \frac{t}{A}\int_b (v_S^2 + w_S^2) ds \qquad X_D = \frac{t}{A}\int_b (v_D^2 + w_D^2) ds$$
$$X^{II}_S = \frac{t}{I_{II}}\int_b u_{II}(v_S^2 + w_S^2) ds \qquad X^{II}_D = \frac{t}{I_{II}}\int_b u_{II}(v_D^2 + w_D^2) ds$$
$$X^I_{SD} = \frac{t}{I_I}\int_b u_I (v_S v_D + w_S w_D) ds \tag{6}$$

Once the functions $\phi_S(x)$ and $\phi_D(x)$ are known, it is possible to obtain formulae to provide bifurcation stress estimates. One writes $\phi_S(x)$ and $\phi_D(x)$ in the form

$$\phi_S(x) = a_S\bar{\phi}(x) \qquad \phi_D(x) = a_D\bar{\phi}(x) \tag{7}$$

where (i) a_S and a_D are deformation mode amplitudes and (ii) $\bar{\phi}(x)$ is a unit shape function describing (exactly or approximately) their longitudinal variation. Introducing Eq. (7) in Eq. (5) and applying Galerkin's method, one is led to the eigenvalue problem

$$\begin{bmatrix} K_S-\lambda_b\bar{P}X_S^* & -\lambda_b\bar{M}\cos\alpha X_{SD}^I \\ -\lambda_b\bar{M}\cos\alpha X_{SD}^I & K_D-\lambda_b\bar{P}X_D^* \end{bmatrix}\begin{Bmatrix} a_S \\ a_D \end{Bmatrix} = \begin{Bmatrix} 0 \\ 0 \end{Bmatrix} \tag{8}$$

with

$$K_S = EC_S\left(\frac{\pi}{L}\right)^2\mu_C + GD_S + B_S\left(\frac{L}{\pi}\right)^2\mu_B \qquad K_D = EC_D\left(\frac{\pi}{L}\right)^2\mu_C + GD_D + B_D\left(\frac{L}{\pi}\right)^2\mu_B \tag{9}$$

$$X_S^* = \bar{P}X_S + \bar{M}\sin\alpha X_S^{II} \qquad X_D^* = \bar{P}X_D + \bar{M}\sin\alpha X_D^{II} \tag{10}$$

where α is the angle between the applied bending moment vector and the cross-section *I-axis* (see Fig. 5(b)). Moreover, parameters μ_B and μ_C are given by (note the change of variable $y = \pi x / L$).

$$\mu_B = \frac{\int_0^\pi \bar{\phi}^2 dy}{\int_0^\pi \bar{\phi}_{,y}^2 dy} \qquad \mu_C = \frac{\int_0^\pi \bar{\phi}_{,yy}^2 dy}{\int_0^\pi \bar{\phi}_{,y}^2 dy} \tag{11}$$

and depend only on the characteristics of function $\bar{\phi}(y)$, *i.e.*, the member support conditions and half-wave number *n*. Expressions for μ_B and μ_C are given in section **5.**, for four support conditions.

Solving Eqs. (8) (eigenvalue problem) analytically leads to the λ_b estimate (in terms of L)

$$\lambda_b = \frac{\eta_1}{2\eta_2} \pm \sqrt{\left(\frac{\eta_1}{2\eta_2}\right)^2 - \frac{K_S K_D}{\eta_2}} \tag{12}$$

where

$$\eta_1 = K_S X_D^* + K_D X_S^* \qquad \eta_2 = X_S^* X_D^* - (\bar{M}\cos\alpha X_{SD}^I)^2 \tag{13}$$

and the plus (minus) sign holds for $\eta_2<0$ (>0). After knowing λ_b, one readily calculates the buckling load $P_b=\lambda_b\bar{P}$ and moment components $M_b^I=\lambda_b\bar{M}\cos\alpha$ and $M_b^{II}=\lambda_b\bar{M}\sin\alpha$. The eigenvector related to λ_b provides the degrees of participation of modes S and D in the *beam-column* DM:

$$a_S = \frac{1}{1-\dfrac{M_b^I X_{SD}^I}{K_D - P_b X_D^*}} \qquad a_D = 1 - a_S \tag{14}$$

The *critical length* L_{cr}, corresponding to the minimum λ_b ($\lambda_{b.min}$), is the relevant root of $d\lambda_b/dL=0$. However, since function $\lambda_b(L)$ is highly non linear (see Eq. (12)), the exact value of this root cannot be determined analytically. However, it was found that expression

$$L_{cr} = \pi \sqrt[8]{\frac{E^2 C_S}{B_S}\left[\frac{C_S}{B_S}\overline{P} + \left(\frac{C_D}{B_D}\cos^2\alpha + \frac{C_S}{B_S}\sin^2\alpha\right)\overline{M}\right]} \sqrt[4]{\frac{\mu_C}{\mu_B}} \tag{15}$$

estimates L_{cr} quite accurately (errors seldom above 2%), provided that the normalisation condition

$$\overline{P} + \overline{M} = 1 \tag{16}$$

is used to determine $\overline{P}$ and $\overline{M}$. Then, introducing Eq. (15) in Eq. (12), one readily obtains $\lambda_{b.min}$.

If $\overline{P}$=1 and $\overline{M}$=0, the above expressions yield *column* L_{cr} and $P_{b.min}$ (=$\lambda_{b.min}$) estimates. Since Eqs. (8) are uncoupled and only the first one (mode S) is relevant and Eqs. (12) and (15) become

$$L_{cr} = \pi \sqrt[4]{\frac{EC_S}{B_S}} \sqrt[4]{\frac{\mu_C}{\mu_B}} \qquad P_{b.min} = \frac{K_{S.cr}}{X_S} = \frac{2\sqrt{EC_S B_S}\sqrt{\mu_C \mu_B} + GD_S}{X_S} \tag{17}$$

where $K_{S.cr}$=K_S(L_{cr}) (see Eq. (9)). They are much simpler than their beam-column counterparts.

If $\overline{P}$=0 and $\overline{M}$=1, on the other hand, one obtains *beam* L_{cr} and $M_{b.min}$ (=$\lambda_{b.min}$) estimates. Although the formulae apply to bending about an *arbitrary* neutral axis (Fig. 5(b_1)), rack-section beams are mostly subjected to *uniaxial* bending, a much simpler case. Then, one has:

(i) In *I-axis beams* (Fig. 5(b_2) - α=0), Eqs. (12) and (15) become

$$L_{cr} = \pi \sqrt[8]{\frac{E^2 C_S C_D}{B_S B_D}} \sqrt[4]{\frac{\mu_C}{\mu_B}} \qquad M_{b.min} = \sqrt{\frac{K_{S.cr} K_{D.cr}}{\left(X_{SD}^I\right)^2}} \tag{18}$$

where $K_{S.cr}$=K_S(L_{cr}) and $K_{D.cr}$=K_D(L_{cr}) (see Eq. (9)). The estimates yielded by these two expressions can be directly compared with those provided by Hancock (1997).

(ii) In *II-axis beams* (Fig. 5(b_3) - $\alpha = -\pi/2$), the DM shape is *symmetric*. Thus, Eqs. (8) are uncoupled and only the first one matters (as in columns). Then, Eqs. (12) and (15) become

$$L_{cr} = \pi \sqrt[4]{\frac{EC_S}{B_S}} \sqrt[4]{\frac{\mu_C}{\mu_B}} \qquad M_{b.min} = \frac{K_{S.cr}}{X_S^{II}} = \frac{2\sqrt{EC_S B_S}\sqrt{\mu_C \mu_B} + GD_S}{X_S^{II}} \tag{19}$$

and their estimates can be directly compared with those provided by Teng *et al*. (2003).

Finally, since the tension flange of *I-axis beams* (case (ii) in Fig. 5(b_2)) practically doesn't move (see Fig. 1(b_2)), one anticipates very close a_S and a_D values ($\approx$ 0.50 each). Since a *beam* applied stress diagram varies between the *I-axis* and *II-axis* bending ones, one can say that the a_D and a_S values are bounded by (i) 0 and $\approx$ 0.50 and (ii) 1 and $\approx$ 0.50, respectively. Moreover, since a *beam-column* stress diagram varies between the *column* and a *beam* ones, one can also say that a_D is either (i) 0 (*II-axis beam-columns*) or (ii) bounded by 0 and $\approx 0.50 a_S$ (*I-axis beam-columns*).

4. Cross-section distortional properties

In order to derive expressions for the cross-section mechanical and geometrical properties, related to modes S and D, one must know the relevant cross-section *displacements* and *transverse bending*

moments. The expressions providing the *warping* ($u_\alpha(s)$), *membrane* ($v_\alpha(s)$) and *flexural* ($w_\alpha(s)$) displacements in an arbitrary wall (element) α ($\alpha = 1\ldots7$, $s_\alpha \le s \le s_{\alpha+1}$) read (see Fig. 6(a))

$$u_\alpha(s) = \frac{1}{2}\boldsymbol{u}_\alpha(\Psi_1 - \Psi_2) + \frac{1}{2}\boldsymbol{u}_{\alpha+1}(\Psi_1 + \Psi_2) \qquad v_\alpha(s) = \boldsymbol{v}_\alpha \Psi_1 \tag{20}$$

$$w_\alpha(s) = \boldsymbol{w}_\alpha \Psi_1 + \frac{1}{2} b_\alpha \boldsymbol{\varphi}_\alpha \Psi_2 - \frac{1}{3K} b_\alpha^2 (\boldsymbol{m}_\alpha \Psi_3 + \boldsymbol{m}_{\alpha+1} \Psi_4) \tag{21}$$

where (i) b_α and K are the wall width and plate bending stiffness and (ii) the shape functions $\Psi_i(\xi)$ ($\xi = (s - s_\alpha) / b_\alpha$, $b_\alpha = s_{\alpha+1} - s_\alpha$) are depicted in Fig. 6(b).

Eqs. (20)-(21) show that u_α, v_α and w_α are linear, constant and cubic functions of s, fully defined by (i) nodal (i_1) *warping displacements* $\boldsymbol{u}_\alpha$, $\boldsymbol{u}_{\alpha+1}$ and (i_2) *transverse moments* $\boldsymbol{m}_\alpha$, $\boldsymbol{m}_{\alpha+1}$, and (ii) wall chord (centre-line) (ii_1) *membrane displacements* $\boldsymbol{v}_\alpha$ and (ii_2) *flexural displacements* $\boldsymbol{w}_\alpha$ and (ii_3) *rotations* $\boldsymbol{\varphi}_\alpha$. For modes S and D, these values are components of vectors ($\alpha = 1\ldots7$).

$$\boldsymbol{u} = \{\gamma \;\; u_2 \;\; u_3 \;\; u_4 \;\; u_4\gamma \;\; u_3\gamma \;\; u_2\gamma \;\; 1\}^T \qquad \boldsymbol{m} = \{0 \;\; 0 \;\; m_3 \;\; m_4 \;\; m_4\gamma \;\; m_3\gamma \;\; 0 \;\; 0\}^T \tag{22}$$

$$\boldsymbol{v} = \{v_l \;\; v_s \;\; v_f \;\; v_w \;\; -v_f\gamma \;\; -v_s\gamma \;\; -v_l\gamma\}^T \qquad \boldsymbol{w} = \{w_l \;\; w_s \;\; w_f \;\; w_w \;\; w_f\gamma \;\; w_s\gamma \;\; w_l\gamma\}^T \tag{23}$$

$$\boldsymbol{\varphi} = \{\varphi_l \;\; \varphi_s \;\; \varphi_f \;\; \varphi_w \;\; -\varphi_f\gamma \;\; -\varphi_s\gamma \;\; -\varphi_l\gamma\}^T \tag{24}$$

where the value of γ enables the distinction between modes S ($\gamma = 1$) and D ($\gamma = -1$). Fig. 7 provides the physical meaning of the above modal vector components, for the cross-section discretisation shown in Fig. 3(a). Since modes S and D exhibit either *symmetric* or *anti-symmetric* displacement and moment diagrams, the unknowns in Eqs. (22)-(24) can be reduced accordingly.

Before determining the mode S and D mechanical properties, on must solve, *numerically*, the *auxiliary* (standard) *eigenvalue problem* defined by Eq. (3)[4], a procedure responsible for the formulae "quasi-analytical" character. However, one must point out that this eigenvalue problem is *analytically defined* in annex (the *explicit expressions* provided make it possible to determine all matrix components). Its solution involves the following steps:

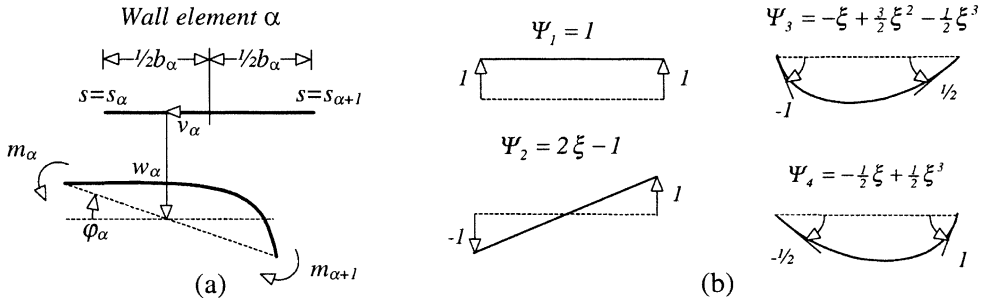

Fig. 6 Wall element α (a) deformed configuration $w_\alpha(s)$ and (b) shape functions $\Psi_i(\xi)$

[4]In 5 wall members, this is done *analytically*, thus leading to "fully analytical" formulae (Silvestre & Camotim 2003).

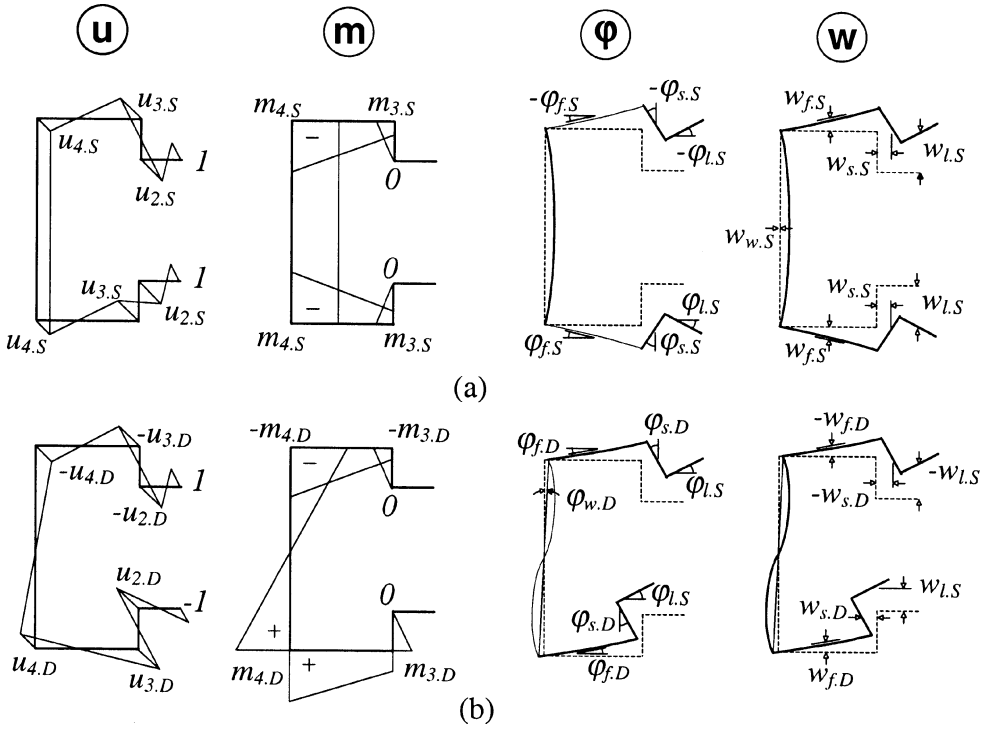

Fig. 7 Distributions/diagrams of **u**, **m**, $\boldsymbol{\varphi}$ and **w** for modes (a) S and (b) D

(I) Determine the *geometrical* and *mechanical parameters*

$$\alpha_f = \frac{b_f}{b_w} \qquad \alpha_s = \frac{b_s}{b_w} \qquad \alpha_l = \frac{b_l}{b_w} \qquad K = \frac{Et^3}{12(1-\nu^2)} \tag{25}$$

(II) Using the components of **F** and $\ddot{\mathbf{w}}$, given in annex, determine matrices

$$\mathbf{M} = -\mathbf{F}^{-1}\ddot{\mathbf{w}} \qquad \mathbf{B} = -\ddot{\mathbf{w}}^T\mathbf{M} \tag{26}$$

(III) Using the components of **C**, also given in annex, solve the 8^{th}*-order* eigenvalue problem

$$(\mathbf{B} - \lambda\mathbf{C})\mathbf{u} = 0 \tag{27}$$

which has four *null* eigenvalues (corresponding to rigid-body deformation modes).

(IV) Determine eigenvectors $\mathbf{u}_S$ and $\mathbf{u}_D$, corresponding to the *two smallest non-null* eigenvalues ($0 < \lambda_S < \lambda_D$), and write their components (*nodal warping displacements*) as in Eq. (22_1).

(V) Evaluate vectors $\mathbf{m}_S$ and $\mathbf{m}_D$, by means of

$$\mathbf{m}_s = \mathbf{M}\,\mathbf{u}_s \qquad \mathbf{m}_D = \mathbf{M}\,\mathbf{u}_D \tag{28}$$

and write their components (*nodal transverse bending moments*) as in Eq. (22_2).

After having the $\mathbf{u}_S$, $\mathbf{u}_D$, $\mathbf{m}_S$, $\mathbf{m}_D$ components, the evaluation of the modal mechanical properties is *fully analytical*. The code MAPLE (WMS 2001) was used to derive expressions for v_l, v_s, v_f, v_w, φ_l, φ_s, φ_f, φ_w, w_l, w_s, w_f, w_w, involving the (i) $\mathbf{u}_S$, $\mathbf{u}_D$, $\mathbf{m}_S$, $\mathbf{m}_D$ components, (ii) cross-section dimensions b_w, b_f, b_s,

b_l, θ, t and (iii) material constants E, ν. The derivation comprises five steps:

(VI) Evaluate the wall chord *membrane displacements* $v_{f.S}$, $v_{w.S}$, $v_{s.S}$, $v_{l.S}$ and $v_{f.D}$, $v_{w.D}$, $v_{s.D}$, $v_{l.D}$

$$v_w = \frac{u_4(1-\gamma)}{b_w} \qquad v_f = \frac{u_3-u_4}{\alpha_f\, b_w} \qquad v_s = \frac{u_2-u_3}{\alpha_s b_w} \qquad v_l = \frac{\gamma-u_2}{\alpha_l b_w} \tag{29}$$

(VII) Evaluate the wall chord *rotations* $\varphi_{f.S}$, $\varphi_{w.S}$, $\varphi_{s.S}$, $\varphi_{l.S}$ and $\varphi_{f.D}$, $\varphi_{w.D}$, $\varphi_{s.D}$, $\varphi_{l.D}$

$$\varphi_w = \frac{v_f(1-\gamma)}{b_w} \qquad \varphi_f = \frac{1}{\alpha_f\, b_w}\left(-\frac{v_f}{\tan\theta}+\frac{v_s}{\sin\theta}+\frac{v_w}{2}(1-\gamma)\right)$$

$$\varphi_s = \frac{v_f-v_l}{\alpha_s b_w \sin\theta} \qquad \varphi_l = \varphi_s + \frac{\alpha_s\, b_w m_3}{6K} \tag{30}$$

(VIII) Evaluate the wall chord *flexural displacements* $w_{f.S}$, $w_{w.S}$, $w_{s.S}$, $w_{l.S}$ and $w_{f.D}$, $w_{w.D}$, $w_{s.D}$, $w_{l.D}$

$$w_w = -\frac{v_f}{2}(1+\gamma) \qquad w_f = \frac{1}{2}\left(\frac{v_f}{\tan\theta}-\frac{v_s}{\sin\theta}+\frac{v_w}{2}(1-\gamma)\right)$$

$$w_s = \frac{v_f+v_l}{2\sin\theta}-\frac{v_s}{\tan\theta} \qquad w_l = -\frac{v_s}{\sin\theta}+\frac{v_l}{\tan\theta}-\frac{1}{2}\varphi_l\alpha_l b_w \tag{31}$$

(IX) Evaluate the cross-section *modal mechanical properties* C_S, B_S, D_S and C_D, B_D, D_D

$$C = \frac{1}{3}b_w t[(2+\gamma)u_4^2+2\alpha_f\,(u_4^2+u_4u_3+u_3^2)+2\alpha_s\,(u_3^2+u_3u_2+u_2^2)+2\alpha_l\,(u_2^2+\gamma u_2+1)]$$

$$B = \frac{1}{3K}b_w[(2+\gamma)m_4^2+2\alpha_f\,(m_4^2+m_4m_3+m_3^2)+2\alpha_s m_3^2]$$

$$D = \frac{2}{3}b_w t^3\left(\alpha_l\varphi_l^2+\alpha_s\varphi_s^2+\alpha_f\varphi_f^2+\frac{1}{2}\varphi_w^2\right) \tag{32}$$

(X) Evaluate the cross-section *geometric stiffness components*

$$X = \frac{b_w t}{15120K^2C}\sum_i X_i \tag{33}$$

(X.1) For the individual modes S and D: X_S, X_D, X_S^{II} and X_D^{II}

$$X_1 = 15120K^2[(v_w^2+w_w^2)U_4+\alpha_f(v_f^2+w_f^2)(U_4+U_3)+$$

$$+\alpha_s(v_s^2+w_s^2)(U_3+U_2)+\alpha_l(v_l^2+w_l^2)(U_2+U_1)]$$

$$X_2 = 84Kb_w^3\left[\alpha_f^4\varphi_f\, m_4(2U_4-U_3)+\alpha_f^4\varphi_f\, m_3(U_4-2U_3)+\alpha_s^4\varphi_s\, m_3(2U_3-U_2)+\frac{1}{2}\varphi_w\, m_4U_4(\gamma-1)\right]$$

$$X_3 = b_w^4[m_4^2U_4(64+62\gamma)+\alpha_f^5m_4^2(35U_4+29U_3)+\alpha_f^5m_3^2(29U_4+35U_3)+$$

$$+\alpha_s^5m_3^2(35U_3+29U_2)+62\alpha_f^5m_4m_3(U_4+U_3)]$$

$$X_4 = 5040K^2b_w[\alpha_f^2\varphi_f\, w_f(U_4-U_3)+\alpha_s^2\varphi_s w_s(U_3-U_2)+\alpha_l^2\varphi_l w_l(U_2-U_1)]$$

$$X_5 = 1260K^2 b_w^2[\alpha_f^3 \varphi_f^2 (U_4 + U_3) + \alpha_s^3 \varphi_s^2 (U_3 + U_2) + \alpha_l^3 \varphi_l^2 (U_2 + U_1) + \varphi_w^2 U_4]$$

$$X_6 = 84Kb_w^2[15(1+\gamma)\, w_w m_4 U_4 + 2\alpha_f^3 w_f\, m_4(8U_4 + 7U_3) +$$

$$+2\alpha_f^3 w_f\, m_3(7U_4 + 8U_3) + 2\alpha_s^3 w_s m_3(8U_3 + 7U_2)]$$

(X.2) For the coupling between modes S and D: X_{SD}^I

$$X_1 = 15120K^2[\alpha_f(v_{f.S}v_{f.D} + w_{f.S}w_{f.D})(U_4 + U_3) + \alpha_s(v_{s.S}v_{s.D} + w_{s.S}w_{s.D})(U_3 + U_2) +$$
$$+\alpha_l(v_{l.S}v_{l.D} + w_{l.S}w_{l.D})(U_2 + U_1)]$$

$$X_2 = 42b_w^3 K[-3\varphi_{w.D}m_{4.S}U_4 + \alpha_s^4(\varphi_{s.S}m_{3.D} + \varphi_{s.D}m_{3.S})(2U_3 - U_2) +$$

$$+\alpha_f^4(\varphi_{f.S}m_{4.D} + \varphi_{f.D}m_{4.S})(2U_4 - U_3) + \alpha_f^4(\varphi_{f.S}m_{3.D} + \varphi_{f.D}m_{3.S})(U_4 - 2U_3)]$$

$$X_3 = 2520K^2 b_w[-w_{w.S}\varphi_{w.D}U_4 + \alpha_f^2(w_{f.S}\varphi_{f.D} + w_{f.D}\varphi_{f.S})(U_4 - U_3) +$$

$$+\alpha_s^2(w_{s.S}\varphi_{s.D} + w_{s.D}\varphi_{s.S})(U_3 - U_2) + \alpha_l^2(w_{l.S}\varphi_{l.D} + w_{l.D}\varphi_{l.S})(U_2 - U_1)]$$

$$X_4 = 1260K^2 b_w^2[\alpha_f^3 \varphi_{f.D}\varphi_{f.S}(U_4 + U_3) + \alpha_s^3 \varphi_{s.D}\varphi_{s.S}(U_3 + U_2) + \alpha_l^3 \varphi_{l.D}\varphi_{l.S}(U_2 + U_1)]$$

$$X_5 = 84Kb_w^2[w_{w.S}m_{4.D}U_4 + \alpha_s^3(w_{s.S}m_{3.D} + w_{s.D}m_{3.S})(8U_3 + 7U_2) +$$

$$+\alpha_f^3(w_{f.S}m_{4.D} + w_{f.D}m_{4.S})(8U_4 + 7U_3) + \alpha_f^3(w_{f.S}m_{3.D} + w_{f.D}m_{3.S})(7U_4 + 8U_3)]$$

$$X_6 = b_w^4[6m_{4.S}m_{4.D}U_4 + 31\alpha_f^5(m_{4.S}m_{3.D} + m_{3.S}m_{4.D})(U_4 + U_3) + \alpha_f^5 m_{4.S}m_{4.D}(35U_4 + 29U_3) +$$

$$+\alpha_f^5 m_{3.S}m_{3.D}(29U_4 + 35U_3) + \alpha_s^5 m_{3.S}m_{3.D}(35U_3 + 29U_2)]$$

Table 1 shows the values of (i) the *pre-buckling nodal axial displacements* U_1-U_4 and (ii) the associated cross-section *C* property, equal to *A*, I_I or I_{II} (cross-sectional area, major and minor moments of inertia) for compression, major or minor axis bending. Recall that (i) the pre-buckling axial displacements are *symmetric* ($U_8=U_1$, $U_7=U_2$, $U_6=U_3$, $U_5=U_4$ - columns and *II-axis* beams: step X.1) or *anti-symmetric* ($U_8=-U_1$, $U_7=-U_2$, $U_6=-U_3$, $U_5=-U_4$ - *I-axis* beams: step X.2) (see Fig. 8) and that (ii) a beam-column always concerns two (compression + uniaxial bending) or three (compression + biaxial bending) diagrams. Note also that the complexity of Eqs. (33) is largely due to their generality. In columns, for instance, because one has $U_1=U_2=U_3=U_4=1$, all (U_i-U_j) terms vanish and Eqs. (33) become much simpler.

Table 1 Steps X: nodal pre-buckling axial displacements and cross-section C property

Step	X	U_4	U_3	U_2	U_1	C
X.1	X_S, X_D	1	1	1	1	A
	X_S^{II}, X_D^{II}	x_G	$x_G - \alpha_f b_w$	$U_3 - \alpha_s b_w \cos\theta$	$U_2 - \alpha_l b_w$	I_{II}
X.2	X_{SD}^I	½ b_w	½ b_w	½ $b_w - \alpha_s b_w \sin\theta$	½ $b_w - \alpha_s b_w \sin\theta$	I_I

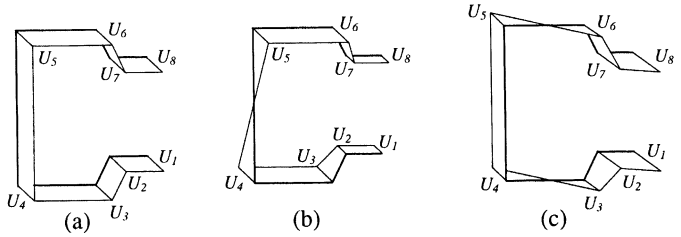

Fig. 8 Nodal pre-buckling axial displacements: (a) column (b) *I-axis* beam (c) *II-axis* beam

Table 2 Column, beam and beam-column geometric stiffness components

Columns	Beams			Beam-columns		
	I-axis	*II-axis*	Any axis	*I-axis*	*II-axis*	Any axis
X_S	X_{SD}^{I}	X_S^{II}	$X_{SD}^{I}, X_S^{II}, X_D^{II}$	X_S, X_D, X_{SD}^{I}	X_S, X_S^{II}	$X_S, X_D, X_{SD}^{I}, X_S^{II}, X_D^{II}$

Finally, Table 2 shows the geometric stiffness components. Note that columns and *II-axis* beams and beam-columns need only mode S properties. In all other cases, both S and D properties are required.

5. End support conditions

As mentioned earlier, four end support conditions are considered in this work: (i) pinned and free-to-warp end sections (PFW), (ii) fixed and warping-prevented end sections (FWP), (iii) one FWP section and the other PFW and (iv) one FWP end section and the other "sliding-fixed" and warping-prevented (SWP). The following *trigonometric* approximation functions $\overline{\phi}(y)$, which (i) satisfy all end support conditions and (ii) were successful used by Bradford & Azhari (1995), in the context of finite strip plate linear stability analyses, have been adopted:

(i) PFW members (in this case, the $\overline{\phi}(y)$ provide the *exact solution* of Eqs. (1))

$$\overline{\phi}(y) = \sin(ny) \tag{34}$$

(ii) FWP members

$$\overline{\phi}(y) = \sin(ny)\sin(y) \tag{35}$$

(iii) FWP-PFW

$$\overline{\phi}(y) = \sin[(n+1)y] + \frac{n+1}{n}\sin(ny) \tag{36}$$

(iv) FWP-SWP members

$$\overline{\phi}(y) = \sin\left[\left(n-\frac{1}{2}\right)y\right]\sin\left(\frac{1}{2}y\right) \tag{37}$$

Introducing Eqs. (34)-(37) in Eq. (11) and integrating w.r.t. y leads to (n is the half-wave number):

(i) PFW members

$$\mu_B = \frac{1}{n^2} \qquad \mu_C = n^2 \tag{38}$$

(ii) FWP members

$$\mu_B = \frac{3(if\ n=1)\ \ or\ \ 2(if\ n\geq 2)}{(n-1)^2+(n+1)^2} \qquad \mu_C = \frac{(n-1)^4+(n+1)^4}{(n-1)^2+(n+1)^2} \tag{39}$$

(iii) FWP-PFW members

$$\mu_B = \frac{(n+1)^2+n^2}{2n^2(n+1)^2} \qquad \mu_C = \frac{1}{2}[(n+1)^2+n^2] \tag{40}$$

(iv) FWP-SWP members

$$\mu_B = \frac{3(if\ n=1)\ \ or\ \ 2(if\ n\geq 2)}{(n-1)^2+n^2} \qquad \mu_C = \frac{2n^4-4n^3+6n^2-4n+1}{(n-1)^2+n^2} \tag{41}$$

Finally, recall that the formulae due to Lau & Hancock (1987), Hancock (1997) and Teng *et al*. (2003) apply to *PFW members* only. Moreover, Davies & Jiang (1998) also derived GBT-based expressions, similar to Eqs. (17) and incorporating Eq. (38), for *PFW columns*. However, since no expressions are given for C_S, D_S, B_S, X_S, their "analytical character" seems quite debatable.

6. A few remarks

After inserting the *mechanical* properties, *geometric stiffness* components and *end support* parameters, the formulae derived in section **3.** provide distortional buckling stress resultant estimates (P_b and/or M_b) and also bifurcation stress diagrams, defined by (compression is positive)

$$\sigma_b = \frac{P_b}{A} - \frac{M_b^I}{I_I} x_{II} + \frac{M_b^{II}}{I_{II}} x_I \tag{42}$$

Knowing the distortional buckling stress resultant, one readily (i) calculates the *participation factors* of modes S and D (a_S and a_D) and (ii) characterises the cross-section deformed configuration. Indeed, multiplying a_S and a_D by the corresponding wall displacement fields (see Eqs. (20)-(21) and Fig. 7) leads to the cross-section deformation related to the distortional buckling mode.

The derived GBT-based formulae also unveil several *novel* and *useful* aspects concerning distortional buckling of *II-axis beam-columns* (bending in the *symmetry* plane):

(i) L_{cr} is *independent* of the axial force/bending moment combination[5]. Indeed, if $\alpha = -\pi / 2$ Eq. (15) is identical to Eqs. (17_1) and (19_1) for any $\overline{P}$ - $\overline{M}$ combination. This result remains practically true also for *exact* L_{cr} values[6].

(ii) The distortional buckling parameter λ_b (Eq. (12)), related to a given combination of axial load and bending moment, can be expressed *exclusively* in terms of the *column* buckling load P_b and

[5]On the basis of a large number of finite strip analyses, Teng *et al.* (2003) reached a similar conclusion.
[6]A minor variation may occur if the *exact* DM configuration includes small contributions from other GBT modes.

beam buckling moment M_b^{II}. In fact, for $\alpha = -\pi/2$, Eq. (12) may be rewritten as

$$\frac{\overline{P}\lambda_b}{P_b} + \frac{\overline{M}\lambda_b}{M_b^{II}} = 1 \tag{43}$$

and corresponds to a linear variation between P_b and M_b^{II}.

It is still worth noting that the GBT-based formulae incorporate genuine folded-plate theory, a feature which (i) accounts for their *accuracy* and *generality* and (ii) makes it possible to clarify (overcome) the assumptions (limitations) of the other distortional buckling formulae. Indeed:

(i) All formulae based on Lau and Hancock's model involve estimating the elastic lateral restraint provided by the web to the "flange-stiffener assembly" (k_x - see Fig. 1(c_1)). Since it is not possible to find exact k_x values, the two extreme cases $k_x = 0$ and $k_x \to \infty$ have been dealt with and the former was adopted. The GBT-based formulae *confirm* that $k_x = 0$ is a correct assumption, since it is shown that the web-flange corner moves by (i_1) $w_{w.S}$ (columns) and (i_2) $a_S w_{w.S} + \frac{1}{2} a_D b_w \varphi_{w.D}$ (*I-axis* beams) - see Fig. 7.

(ii) Numerical simulations provided evidence that, besides rigid-body motions, the compressed flanges may also experience *non-negligible* flexural deformations if the width ratio b_f / b_w is large enough (Lau & Hancock 1987 and Teng *et al.* 2003). Thus, all the formulae based on Lau and Hancock's model need to include an adjustment factor *a*, determined *a priori* and accounting for the flange flexural deformations. As shown in Fig. 7, the GBT-based formulae automatically incorporate this effect (flange components of $\mathbf{m}_S$ and $\mathbf{m}_D$).

(iii) Bambach *et al.* (1998) showed, in the context of C-sections with return lips (similar to rack-sections), that accurate *I-axis* beam buckling stress estimates require the consideration of the *stiffener stress gradient*. In order to improve the formulae derived by Hancock (1997), assuming the stiffeners under *uniform stress*, they proposed the inclusion of an *adjustment factor*. In the case of the GBT-based formulae, which already incorporate the effect the stress gradients acting in every cross-section wall, this issue is automatically accounted for.

7. Application

First, for illustrative purposes, the application of the distortional buckling formulae to members with PFW support conditions is described in great detail. All members have the same geometry and are subjected to (i) uniform compression, (ii) uniaxial bending, (iii) biaxial bending and (iv) combinations of the above. Then, in order to show the versatility of the formulae, they are also applied to members with FWP support conditions. In both cases, (i) all intermediate steps and values are reported and the estimates are compared with "exact" (numerical) results. Since there exist some qualitative differences between the distortional buckling results presented for PFW members and members with other support conditions (FWP, FWP-PFW or FWP-SWP), note that:

(i) All PFW member σ_b estimates are *minimum values*, *i.e.*, (i_1) concern members with lengths $L = nL_{cr}$, (L_{cr} yielded by Eq. (15)) and (i_2) correspond to critical buckling modes with *n* half-waves ($n=1$ if $L=L_{cr}$). This is illustrated in Fig. 9(a): the buckling curves for individual modes with different *n* values exhibit equally-spaced *identical* minimum values $\sigma_{b.min}$. Moreover, the "all mode curve" is just a superposition of the individual curve lower parts. This means that the critical DM always *coincides with an individual mode*.

(ii) In FWP, FWP-PFW or FWP-SWP members, on the other hand, the individual mode curves

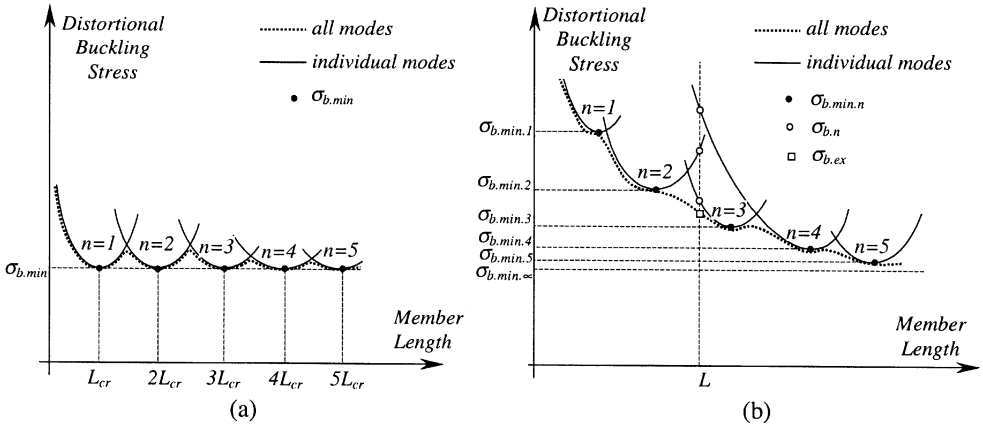

Fig. 9 Distortional buckling curves for (a) PFW and (b) FWP members

exhibit equally-spaced but *different* minimum values $\sigma_{b.min.n}$ (value decreasing with n), as illustrated in Fig. 9(b) (FWP member). Moreover, the all mode curve lies below the superposition of the individual curve lower parts, which means that the critical DM often *combines more than one individual mode*. Thus, it makes no sense to talk about "the minimum bifurcation stress value" and the formulae are used to estimate distortional bifurcation stresses for a member (ii_1) with a given *length* L and (ii_2) buckling in mode with a given *half-wave number* n ($\sigma_{b.n}$). The critical buckling stress estimate is then given by $\sigma_b = \min\{\sigma_{b.1}; \sigma_{b.2}; \sigma_{b.3}; \sigma_{b.4};...\}$ and tends to slightly overestimate the exact value. These concepts are illustrated in Fig. 9(b): the formulae yield $\sigma_b=\sigma_{b.3}$ (lowest white circle), which overestimates the exact value (white square). This means that the critical DM includes participations of, at least, individual modes with 2 and 3 half-waves.

The rack-section geometry selected to illustrate the application of the formulae is given by b_w=100 mm, b_f = 40 mm, b_s=20 mm, b_l=20 mm, t=1.5 mm, θ = 45º and the material properties are E=200 GPa and ν = 0.3. First, one performs the cross-section analysis, comprising the ten steps described in section **4.**. The values of the relevant quantities involved read (see Fig. 10):

(i) Geometrical and mechanical parameters (step I)

$$\alpha_f = 0.5 \qquad \alpha_s = 0.125 \qquad \alpha_l = 0.125 \qquad K = 61813 \text{ Nmm}$$

(ii) Matrices **M**, **B** and **C**, defining the auxiliary eigenvalue problem (steps II-III)

$$\left\{ \underbrace{\begin{bmatrix} 4.11 & -1.71 & -5.35 & 3.32 & -0.53 & 0.34 & -0.08 & -0.08 \\ & 1.19 & 1.49 & -1.02 & -0.12 & 0.34 & -0.09 & \\ & & 8.11 & -4.90 & 1.28 & -1.32 & & \\ & & & 3.02 & -1.05 & & & \\ & & & & & & & \\ & & & & & & & \\ & & & & & & & \\ sym. & & & & & & sym. & \end{bmatrix}}_{\mathbf{B}} \times 10^{-2} - \lambda \cdot \underbrace{\begin{bmatrix} 10 & 5 & 0 & 0 & 0 & 0 & 0 & 0 \\ & 20 & 5 & 0 & 0 & 0 & 0 & \\ & & 30 & 10 & 0 & 0 & & \\ & & & 70 & 25 & & & \\ & & & & & & & \\ & & & & & & & \\ & & & & & & & \\ sym. & & & & & & sym. & \end{bmatrix}}_{\mathbf{C}} \right\} \times \underbrace{\begin{Bmatrix} u_1 \\ u_2 \\ u_3 \\ u_4 \\ u_5 \\ u_6 \\ u_7 \\ u_8 \end{Bmatrix}}_{\mathbf{u}} = \begin{Bmatrix} 0 \\ 0 \\ 0 \\ 0 \\ 0 \\ 0 \\ 0 \\ 0 \end{Bmatrix}$$

(iii) Nodal warping displacements, *i.e.*, components of $\mathbf{u}_S$ and $\mathbf{u}_D$ (step IV)

$$\lambda_S = 4.83\times10^{-4}\ \mathrm{N/mm}^6$$

$$\mathbf{u}_S = \{1.0\ -1.716\ 1.287\ -0.208\ -0.208\ 1.287\ -1.716\ 1.0\}(\mathrm{mm})$$

$$\lambda_D = 14.11\times10^{-4}\ \mathrm{N/mm}^6$$

$$\mathbf{u}_D = \{-1.0\ 1.110\ -0.733\ 0.313\ -0.313\ 0.733\ -1.110\ 1.0\}(\mathrm{mm})$$

(iv) Nodal transverse bending moments, *i.e.*, components of $\mathbf{m}_S$ and $\mathbf{m}_D$ (step V)

$$\mathbf{m}_S = \{0\ \ 0\ \ -0.185\ \ -6.084\ \ -6.084\ \ -0.185\ \ 0\ \ 0\}(\mathrm{Nmm/mm}^2)$$
$$\mathbf{m}_D = \{0\ \ 0\ \ 1.745\ \ 9.072\ \ -9.072\ \ -1.745\ \ 0\ \ 0\}(\mathrm{Nmm/mm}^2)$$

(v) Modal displacements and rotations (steps VI-VIII)

Mode S (γ= 1)

$v_{w.S}$ = 0	$\varphi_{w.S}$ = 0	$w_{w.S}$ = -0.0374 mm/mm
$v_{f.S}$ = 0.0374 mm/mm	$\varphi_{f.S}$ = -0.00624 rad/mm	$w_{f.S}$ = 0.1249 mm/mm
$v_{s.S}$ = -0.1502 mm/mm	$\varphi_{s.S}$ = -0.00696 rad/mm	$w_{s.S}$ = 0.2726 mm/mm
$v_{l.S}$ = 0.1358 mm/mm	$\varphi_{l.S}$ = -0.00697 rad/mm	$w_{l.S}$ = 0.4178 mm/mm

Mode D (γ= -1)

$v_{w.D}$ = 0.0063 mm/mm	$\varphi_{w.D}$ = -0.00052 rad/mm	$w_{w.D}$ = 0
$v_{f.D}$ = -0.0262 mm/mm	$\varphi_{f.D}$ = 0.00407 rad/mm	$w_{f.D}$ = -0.0752 mm/mm
$v_{s.D}$ = 0.0922 mm/mm	$\varphi_{s.D}$ = 0.00561 rad/mm	$w_{s.D}$ = -0.1853 mm/mm
$v_{l.D}$ = -0.1055 mm/mm	$\varphi_{l.D}$ = 0.00571 rad/mm	$w_{l.D}$ = -0.2930 mm/mm

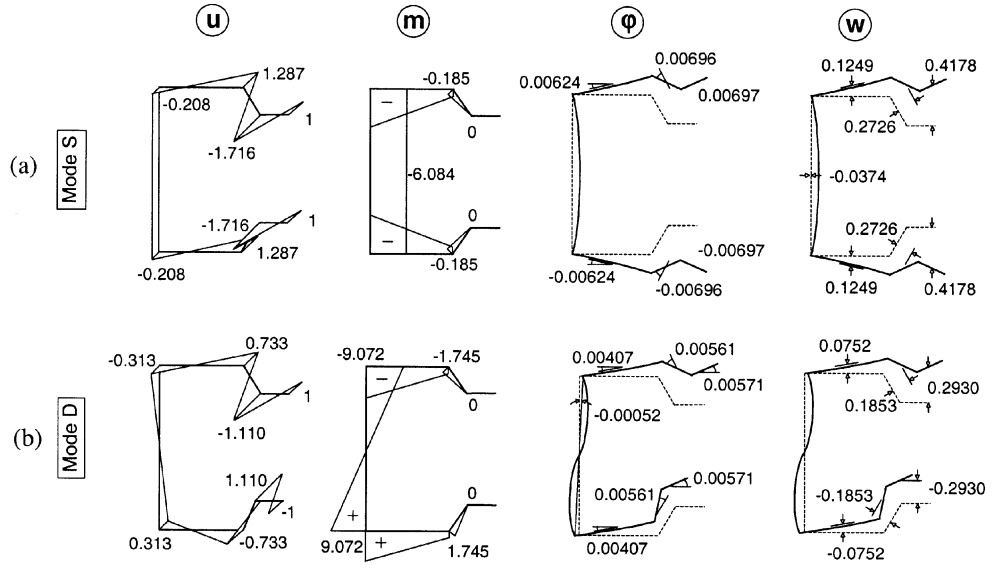

Fig. 10 Displacements and bending moments associated with (a) mode S and (b) mode D

(vi) Cross-section modal mechanical properties (step IX)

$$C_S = 156.180 \text{ mm}^4 \qquad B_S = 7.6349\times10^{-2} \text{ N/mm}^2 \qquad D_S = 8.8134\times10^{-3} \text{ mm}^2$$
$$C_D = 62.761 \text{ mm}^4 \qquad B_D = 8.8694\times10^{-2} \text{ N/mm}^2 \qquad D_D = 4.6361\times10^{-3} \text{ mm}^2$$

(vii) Cross-section geometric stiffness components (step X)

$$X_S = 5.7443\times10^{-2} \qquad X_D = 2.4364\times10^{-2}$$
$$X_{SD}^{I} = -8.8915\times10^{-4} \text{ mm}^{-1} \qquad X_S^{II} = -2.5320\times10^{-3} \text{ mm}^{-1} \qquad X_D^{II} = -1.3388\times10^{-3} \text{ mm}^{-1}$$
$$A = 390 \text{ mm}^2 \qquad x_G = 23.26 \text{ mm} \qquad I_I = 613720 \text{ mm}^4 \qquad I_{II} = 235728 \text{ mm}^4$$

7.1. PFW members

The (i) L_{cr}, (ii) $P_{b.min}$ and/or $M_{b.min}$ and (iii) a_S and a_D estimates concerning PFW columns, beams and beam-columns are presented next, together with the *exact* L_{cr} and $P_{b.min}$ and/or $M_{b.min}$ values (inside square brackets), obtained from GBT analyses incorporating all deformation modes (global, distortional and local-plate). Since the results are independent of n, n=1 is adopted for simplicity. Figs. 11(a_1)-(a_4) show four applied stress diagrams (values in MPa), corresponding to the bifurcation of one column, two beams and one beam-column. Combining the modal S and D quantities, through a_S and a_D, one obtains the *buckling mode* quantities, depicted (i) in Fig. 11(b), for the *I-axis* beam, and (ii) in Fig. 10(a), for the column, *II-axis* beam and beam-column (a_S=1).

All the relevant distortional buckling results are:

(i) Column (Figs. 11(a_1) and 10(a))

$$L_{cr} = 447 \text{ mm}[446] \qquad P_{b.min} = 65.5 \text{ kN}[65.3] \qquad \{a_S;\ a_D\} = \{1;0\}$$

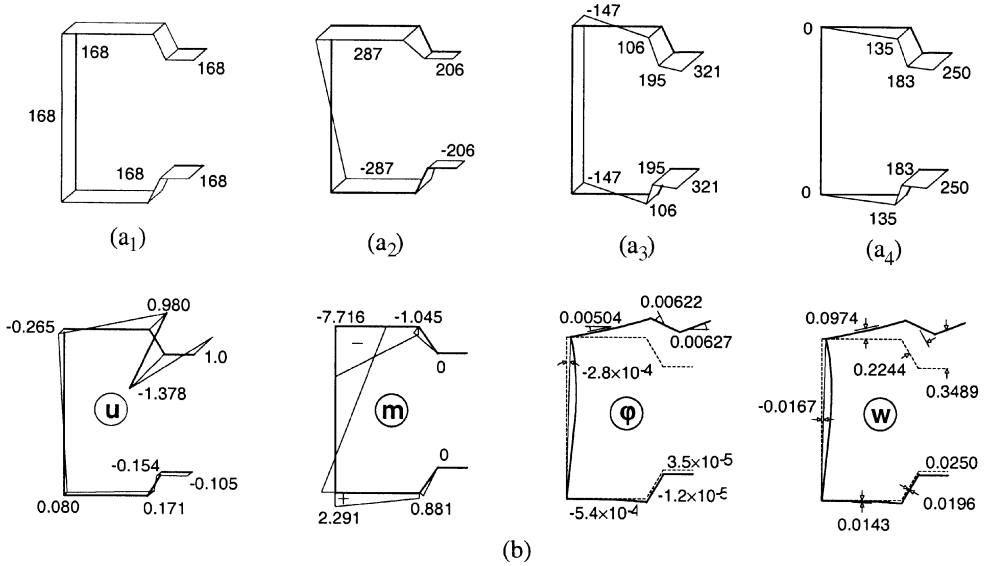

Fig. 11 (a) Bifurcation (a_1) column (a_2) *I-axis* beam (a_3) *II-axis* beam (a_4) *II-axis* beam-column stress distributions and (b) *I-axis* beam DM quantities

(ii) *I-axis* beam (α = 0 - Figs. 11(a_2) and 11(b))

$$L_{cr} = 391 \text{ mm}[391] \qquad M_{b.min} = 3530 \text{ kNmm}[3465]$$
$$\{a_S;\ a_D\} = \{0.447;0.553\}$$

(iii) *II-axis* beam ($\alpha = -\pi/2$ - Figs. 11(a_3) and 10(a))

$$L_{cr} = 447 \text{ mm}[430] \qquad P_{b.min} = 1487 \text{ kNmm}[1403] \qquad \{a_S;\ a_D\} = \{1;0\}$$

(vi) *II-axis* beam-column (P=4 kN + M = 104.1 kNmm - Figs. 11(a_1) and 10(a))

$$\overline{P} = 0.037 \text{ N} \qquad \overline{M} = 0.963 \text{ Nmm}$$
$$L_{cr} = 447 \text{ mm}[440] \qquad \lambda_{b.min} = 824743$$
$$P_{b.min} = 30.5 \text{ kN}[29.8] \qquad M_{b.min} = 794 \text{ kNmm}[776] \qquad \{a_S;\ a_D\} = \{1;0\}$$

The observation of this set of results leads to the following remarks:

(i) The GBT-based formulae estimates are quite accurate in all cases.

(ii) Members subjected to uniform compression and/or *II-axis* bending:

(ii.1) The L_{cr} (exact and approximate) values are practically identical for the column, beam and beam-column, which confirms the *independence of* L_{cr} (see section **6.**).

(ii.2) Knowing $P_{b.min}$=65.5 kN, $M_{b.min}$=1487 kNmm and $\overline{P}$=0.037, $\overline{M}$=0.963, Eq. (43) can be readily used to determine the corresponding *beam-column* parameter λ_b,

$$\frac{0.037\lambda_{b.min}}{65500} + \frac{0.963\lambda_{b.min}}{1487000} = 1 \quad \Leftrightarrow \quad \lambda_{b.min} = 824743 \tag{44}$$

This confirms that $P_{b.min}$ and $M_{b.min}$ provide all the data required to obtain any λ_b.

7.2. FWP members

For FWP members with length L=800 mm, determines first the n minimising the bifurcation stress (*i.e.*, the L_{cr} minimising $K_{S.n}$ and $K_{D.n}$ - see Fig. 9(b)). Then, one obtains estimates for (i) P_b and/or M_b and (ii) a_S and a_D. The relevant values involved in these procedures are presented next (the minimising n is underlined and the *exact* P_b and/or M_b is again inside square brackets):

(i) FWP members

n = 1	μ_C = 4	μ_B = 0.75	$K_{S.1}$ = 6318 N	$K_{D.1}$ = 5445 N
$\underline{n = 2}$	μ_C = 8.2	μ_B = 0.20	$\underline{K_{S.2} = 5618 \text{ N} < K_{S.1}}$	$\underline{K_{D.2} = 3094 \text{ N} < K_{D.1}}$
n = 3	μ_C = 13.6	μ_B = 0.10	$K_{S.3} = 7724 \text{ N} > K_{S.2}$	$K_{D.3} = 3564 \text{ N} > K_{D.2}$

(i.1) Column

$$P_b = 97.8 \text{ kN } [98.9] \qquad \{a_S;\ a_D\} = \{1;0\}$$

(i.2) *I-axis* beam (α = 0)

M_b = 4689 kNmm [4701] $\{a_S; a_D\}$ = {0.604;0.396}

(i.3) *II-axis* beam (α = -π / 2)

M_b = 2219 kNmm [2249] $\{a_S; a_D\}$ = {1;0}

(i.4) *I* + *II-axis* beam-column (α = -π / 4, P = 4 kN + M = 104.1 kNmm)

$\overline{P}$ = 0.037 N $\overline{M}$ = 0.963 Nmm λ_b = 1267343
P_b = 46.9 kN[47.5] M_b = 1220 kNmm[1233] $\{a_S; a_D\}$ = {0.891;0.109}

8. Validation

In order to assess the accuracy and range of validity of the derived formulae, an extensive parametric study was carried out. Its results, given in Tables 3-6 (PFW members) and 7-8 (FWP members), concern columns, beams and beam-columns with several geometries (E=200 GPa and ν = 0.3). The GBT-based estimates are compared with exact results $\sigma_{b.ex}$ and, when possible, also with values yielded

Table 3 PFW columns (b_l = 30 mm, t = 1 mm)

Dimensions (mm)				Exact	Lau & Hancock (1987)		GBT-based	
b_w	b_f	b_s	θ	$\sigma_{b.ex}$	$\sigma_{b.min}$	$\sigma_{b.min}/\sigma_{b.ex}$	$\sigma_{b.min}$	$\sigma_{b.min}/\sigma_{b.ex}$
60	40	10	90°	137	140	1.02	137	1.00
90				116	118	1.02	115	0.99
60	40	15	90°	179	179	1.00	181	1.01
90				150	151	1.01	151	1.01
60	60	10	90°	97	99	1.02	98	1.01
90				86	85	0.99	86	1.00
120				76	74	0.97	75	0.99
60	60	15	90°	130	129	0.99	132	1.02
90				114	111	0.97	115	1.01
120				100	97	0.97	100	1.00
60	40	10	45°	82	90	1.10	82	1.00
90				72	77	1.07	70	0.97
60	40	15	45°	99	108	1.09	99	1.00
90				86	93	1.08	85	0.99
60	60	10	45°	60	62	1.03	60	1.00
90				55	52	0.95	54	0.98
120				49	46	0.94	48	0.98
60	60	15	45°	74	79	1.07	75	1.01
90				66	68	1.03	66	1.00
120				60	59	0.98	60	1.00
100	21	5[8]	90°	128	40	0.31	137	1.07
					Mean[9]	1.02		1.00
					Sd.dev.[9]	0.05		0.01

Table 4 PFW *I-axis* beams (b_l = 30 mm, t = 1 mm)

Dimensions (mm)				Exact	Hancock (1997)		GBT-based	
b_w	b_f	b_s	θ	$\sigma_{b.ex}$	$\sigma_{b.min}$	$\sigma_{b.min}/\sigma_{b.ex}$	$\sigma_{b.min}$	$\sigma_{b.min}/\sigma_{b.ex}$
60	40	10	90°	232	231	1.00	240	1.03
90				182	188	1.03	185	1.02
60	40	15	90°	379	357	0.94	411	1.08
90				271	278	1.03	283	1.04
60	60	10	90°	156	143	0.92	168	1.08
90				128	120	0.94	132	1.03
120				112	106	0.95	114	1.02
60	60	15	90°	258	221	0.86	270	1.05
90				193	175	0.91	204	1.06
120				164	151	0.92	169	1.03
60	40	10	45°	121	140	1.16	123	1.02
90				102	116	1.14	101	0.99
60	40	15	45°	167	182	1.09	174	1.04
90				133	140	1.05	134	1.01
60	60	10	45°	86	94	1.09	89	1.03
90				74	78	1.05	74	1.00
120				67	68	1.01	66	0.99
60	60	15	45°	121	128	1.06	128	1.06
90				98	104	1.06	101	1.03
120				87	91	1.05	88	1.01
					Mean	1.01		1.03
					Sd.dev.	0.08		0.03

by the Lau & Hancock (1987), Hancock (1997) and Teng *et al*. formulae.

All the values displayed in Tables 3 (columns) and 4 (*I-axis* beams) correspond to the distortional bifurcation compressive stress (in MPa) acting on the flange-stiffener corner (node 6 in Fig. 3(a)). The analysis of these results shows that:

(i) The GBT-based estimates are consistently quite accurate. Indeed, the average and standard deviation of the $\sigma_{b.min}/\sigma_{b.ex}$ values read 1.00 and 0.01 (columns) and 1.03 and 0.03 (*I-axis* beams). Moreover, only in two cases does the error exceed 6%.

(ii) For $\theta = 90^o$, Lau and Hancock's formulae yield *column* estimates as accurate as the GBT-based ones (both "evenly distributed" in the "close vicinity" of 1.0[7]). However, note that, unlike the GBT-based formulae, Lau and Hancock's formulae are not valid in the case of high web slenderness. The last line in Table 3 illustrates this statement: since $b_w / b_f \approx 5$, the web rotational stiffness becomes negative and Lau and Hancock's formulae "break down", leading to $\sigma_{b.min}/\sigma_{b.ex}$=0.31 (the GBT-based estimate is $\sigma_{b.min}/\sigma_{b.ex}$ = 1.07).

(iii) For $\theta = 45^o$ (sloping mid-stiffeners), on the other hand, Lau and Hancock's column estimates are

[7]All the cross-section dimensions considered here were taken from Lau (1988). These conclusions may not remain valid for columns with different cross-sections, as happened for channel columns (Silvestre & Camotim 2003).

[8]For this cross-section geometry, one has b_l=b_s=5 mm.

[9]These values do not include the last line, which contains the "meaningless" $\sigma_{b.min}/\sigma_{b.ex}$=0.31 estimate.

Table 5 PFW *II-axis* beams (b_l = 30 mm, $\theta = 90^o$)

Dimensions (mm)				Exact	Teng *et al.* (2003)		GBT-based	
b_w	b_f	b_s	t	$M_{b.ex}$	$M_{b.min}$	$M_{b.min}$ / $M_{b.ex}$	$M_{b.min}$	$M_{b.min}$ / $M_{b.ex}$
60	40	10	1.0	598	622	1.04	612	1.02
90				581	592	1.02	590	1.02
120				576	582	1.01	587	1.02
60	40	15	1.0	846	880	1.04	874	1.03
90				821	829	1.01	845	1.03
120				815	790	0.97	854	1.05
60	60	10	1.0	671	698	1.04	702	1.05
90				651	671	1.03	674	1.04
120				639	659	1.03	659	1.03
150				636	649	1.02	662	1.04
60	60	15	1.0	965	1004	1.04	1020	1.06
90				938	957	1.02	981	1.05
120				922	931	1.01	965	1.05
150				917	908	0.99	957	1.04
60	60	15	1.5	2265	2356	1.04	2384	1.05
90				2209	2253	1.02	2304	1.04
120				2178	2200	1.01	2245	1.03
150				2174	2174	1.00	2230	1.03
					Mean	1.02		1.04
					Sd.dev.	0.02		0.01

less accurate and more scattered than the GBT-based ones.

(iv) All GBT-based *I-axis beam* estimates are slightly unconservative (maximum error of 8% and 6%, for beams with orthogonal and inclined mid-stiffeners). Moreover, the estimates tend to be less accurate for shorter webs and longer flanges and/or stiffeners. The exact results showed that this tendency is due to the influence of the torsion mode.

(v) Hancock's *I-axis* beam estimates[10] are considerably less accurate and more scattered than the GBT-based ones. The errors reach 14% (safe side) and 16% (unsafe side).

Table 5 shows $M_{b.min}$ values concerning *II-axis* beams with cross-section geometries taken from Teng *et al.* (2003) (all with $\theta = 90^o$). One notes that:

(i) Although both the GBT-based and Teng's formulae yield accurate results, (i_1) the GBT-based predictions are a bit more on the unsafe side (averages of 1.04 and 1.02), while (i_2) Teng's estimates are slightly more scattered (standard deviations of 0.02 and 0.01). Nevertheless, one must mention that the accuracy of Teng's estimates is mostly due to an adjustment factor a, which must be determined for each cross-section geometry (if these formulae are to be used for design purposes, a *pre-determined a* value will be imperative).

(ii) The fact that Teng's formulae requires (ii_1) incrementation w.r.t. L (to find L_{cr}) and (ii_2) iteration w.r.t. the rotational stiffness k_ϕ (k_ϕ is L_{cr}-dependent) constitutes a major drawback for design applications. Based on the newly unveiled "L_{cr} independence of the compression-bending combination"

[10]Results obtained using the factor proposed by Bambach *et al.* (1998) to account for the stiffener stress gradient.

Table 6 PFW beam-columns (b_w= 120 mm, b_f = 60, b_s= 15, b_l=30, t=1.5, θ = 90°)

	I-axis beam-columns (e_{II})			*II-axis* beam-columns (e_I)				
	Exact	GBT-based		Exact	Teng *et al.* (2003)		GBT-based	
e	$P_{b.ex}$	$P_{b.min}$	$P_{b.min}/P_{b.ex}$	$P_{b.ex}$	$P_{b.min}$	$P_{b.min}/P_{b.ex}$	$P_{b.min}$	$P_{b.min}/P_{b.ex}$
0	78.0	77.5	0.99	78.0	77.8	1.00	77.5	0.99
1	77.9	77.8	1.00	75.3	75.2	1.00	74.9	0.99
2	77.8	78.0	1.00	72.9	72.7	1.00	72.5	0.99
5	77.0	77.8	1.01	66.5	66.2	1.00	66.1	0.99
10	74.3	75.3	1.01	57.9	57.6	0.99	57.6	0.99
15	70.7	71.8	1.02	51.2	51.0	1.00	51.1	1.00
20	66.9	68.0	1.02	45.9	45.7	1.00	45.9	1.00
25	63.2	64.3	1.02	41.6	41.4	1.00	41.6	1.00
30	59.8	60.8	1.02	38.0	37.9	1.00	38.1	1.00
40	53.8	54.8	1.02	32.4	32.3	1.00	32.5	1.00
60	44.5	45.4	1.02	25.0	25.0	1.00	25.2	1.01
90	35.2	36.0	1.02	18.8	18.6	0.99	18.9	1.01
130	27.5	28.1	1.02	13.9	14.0	1.01	14.1	1.01
180	21.6	22.1	1.02	10.5	10.6	1.01	10.7	1.02
		Mean	1.01		Mean	1.00		1.00
		Sd.dev.	0.01		Sd.dev.	0.01		0.01

(see section **6.**), the authors found that Teng's formulae can be used with the L_{cr} value yielded by Lau & Hancock (1987) *rack-section column formula, i.e.*,

$$L_{cr} = 4.80\left(\frac{I_{wc}b_w}{t^3}\right)^{0.25} \tag{45}$$

where I_{wc} is a geometrical property of the "flange-stiffener assembly". By eliminating the incremental-iterative procedure, with no loss of accuracy, the use of Eq. (45) makes Teng's formulae much more appealing.

Table 6 deals with PFW *beam-columns* (i) having cross-section dimensions b_w=120 mm, b_f = 60, b_s=15, b_l=30, t=1.5, θ = 90° and (ii) acted by an eccentric compressive load (*I* and *II-axis* eccentricities e_I and e_{II} - see Fig. 5(b)). The tabulated results show that the GBT-based estimates (i) are quite accurate in all cases and, for the *II-axis* beam-columns, (ii) match perfectly the high accuracy of Teng's formulae (using Eq. (45) to obtain L_{cr} proved again to be very beneficial).

Finally, Tables 7 (columns) and 8 (*I-axis* beams) concern FWP members with several cross-section geometries and the GBT-based estimates are compared only with exact GBT values (no other distortional buckling formulae available). For validation purposes, all the columns selected have been taken from Lau (1988), who analysed them using the spline finite strip method[11]. The estimates are minimum values, obtained after applying the GBT-based formulae for n=1, 2, 3, ... (the minimising n values are also indicated). One notes that:

(i) The GBT-based formulae continue to provide quite accurate estimates in all cases: (i_1) the σ_b/

[11]The GBT estimates and exact values were obtained after "replacing" the web-flange and flange-stiffener corners by larger width values (corner radius values added to the width values). Although Lau assumed "fictitious" 45°-inclined corner finite strips, the exact GBT values virtually coincide with the spline finite strip results.

Table 7 FWP columns

Dimensions (mm)							Exact		GBT-based	
L	b_w	b_f	b_s	b_l	t	θ	n	$\sigma_{b.ex}$	σ_b	$\sigma_b/\sigma_{b.ex}$
800	79	35.3	16.2	26.8	1.652	90°	2	479	499	0.96
1300							3	410	409	1.00
1500							3	391	385	1.02
1700							4	385	379	1.02
1900							4	374	368	1.02
800	78.6	35.3	16.4	27.05	1.982	90°	2	570	581	0.98
1300							3	490	483	1.01
1500							4	487	481	1.01
1900							5	465	459	1.01
800	82.4	31.4	14.9	29.25	2.395	90°	2	672	660	1.02
1100							3	620	608	1.02
1500							4	587	576	1.02
1700							5	580	569	1.02
800	78.6	35.3	16.4	27.05	1.982	45°	2	292	299	0.98
1300							4	264	270	0.98
1500							4	260	264	0.98
800	82.4	31.4	14.9	29.25	2.395	45°	3	372	386	0.96
1100							4	345	356	0.97
1500							5	330	339	0.97
									Mean	1.00
									Sd.dev.	0.02

$\sigma_{b.ex}$ average and standard deviation read now 1.00 and 0.02 (columns) and 0.97 and 0.03 (*I-axis* beams) and (i_2) the error never exceeds 4% (columns) and 7% (*I-axis* beams).

(ii) Clearly, the less accurate *I-axis* beam estimates concern the shorter beam lengths (two or three half-wave DM). Exact GBT analyses show that this is due to web and/or flange flexural deformation (local-plate) effects, which are not fully accounted for by the formulae.

9. Conclusions

GBT-based analytical formulae to estimate distortional critical lengths and buckling stress resultants in rack-section cold-formed steel members were derived. Since the formulae incorporate *folded-plate theory* concepts, they automatically account for cross-section (i) distortion and (ii) flexural deformation effects (partially). They apply to members with the following characteristics:

(i) Arbitrarily inclined mid-stiffeners.

(ii) Subjected to any combination of uniform compression and uni or biaxial bending.

(iii) Four end support conditions: (iii_1) PFW, (iii_2) FWP, (iii_3) FWP-PFW and (iii_4) FWP-SWP.

Following a very brief overview of the second-order GBT formulation, the paper described and discussed the various steps involved in deriving distortional buckling formulae for rack-section beam-columns (columns and beams are special cases). These formulae are expressed in terms of (i) cross-

Table 8 FWP *I-axis* beams

Dimensions (mm)							Exact		GBT-based	
L	b_w	b_f	b_s	b_l	t	θ	n	$\sigma_{b.ex}$	σ_b	$\sigma_b/\sigma_{b.ex}$
800	79	35.3	16.2	26.8	1.652	90°	2	707	750	0.94
1300							3	714	729	0.98
1500							4	712	719	0.99
1700							4	711	710	1.00
1900							5	710	708	1.00
800	78.6	35.3	16.4	27.05	1.982	90°	2	893	941	0.95
1300							4	906	953	0.95
1500							4	884	907	0.97
1900							5	885	880	1.01
800	82.4	31.4	14.9	29.25	2.395	90°	3	1090	1121	0.97
1100							3	1073	1115	0.96
1500							5	1045	1065	0.98
1700							5	1047	1040	1.01
800	78.6	35.3	16.4	27.05	1.982	45°	3	413	433	0.95
1300							4	405	431	0.94
1500							5	402	424	0.95
800	82.4	31.4	14.9	29.25	2.395	45°	3	500	536	0.93
1100							4	500	532	0.94
1500							6	501	527	0.95
									Mean	0.97
									Sd.dev.	0.03

section distortional mechanical and geometrical properties, (ii) two parameters depending only on the end support conditions and (iii) the member length. A key issue was the determination of "quasi-analytical" expressions to obtain the above distortional properties, which are written exclusively in terms of (i) the cross-section dimensions and material properties and (ii) quantities yielded by the numerical solution of an analytically defined auxiliary eigenvalue problem. It is worth noting that these GBT-based distortional buckling formulae are particularly well suited for design purposes. Indeed, (i) they are easy to program (including the solution of the auxiliary eigenvalue problem) and (ii) their use requires no specific knowledge about distortional buckling.

The paper also included a few remarks concerning (i) qualitative comparisons between the derived formulae and other available distortional buckling formulae and also (ii) novel aspects related to the distortional buckling behaviour of rack-section beam-columns, which were unveiled by the GBT-based approach employed in this work.

The application of the GBT-based formulae was illustrated in considerable detail, as all the intermediate steps and values involved in the analysis of several columns, beams and beam-columns were reported and physically interpreted. Finally, the accuracy and range of validity of the distortional buckling formulae were assessed by means of an extensive parametric study, in which the GBT-based estimates were compared with (i) exact GBT results and, when possible (PFW members only), also with (ii) values yielded by the distortional buckling formulae previously developed by Lau & Hancock, Hancock and Teng *et al.* Columns, beams and beam-columns with several cross-section dimensions

and shapes (orthogonal and sloping mid-stiffeners) were considered and it was possible to reach the following main conclusions:

(i) The GBT-based formulae consistently yield accurate estimates in all the cases dealt with (numerous applied stress diagrams and four support conditions). Indeed, the majority of the estimate errors fell inside the 2% range and only very few of them exceeded 5%.

(ii) Whenever the formulae due to Lau & Hancock, Hancock and Teng *et al.* were applicable (some PWF members), the GBT-based formulae were shown to yield, at least, equally accurate estimates. Moreover, note that none of the previous formulae is valid for (ii_1) columns with very slender webs and (ii_2) *I-axis* beam-columns (all these cases are routinely covered by the derived distortional buckling formulae).

References

Bambach, M., Merrick, J. and Hancock G.J. (1998), "Distortional buckling formulae for thin-walled channel and Z-sections with return lips", *Proc. of 14th Int. Specialty Conf. on Cold-Formed Steel Structures*, St. Louis, October 15-16, 21-37.

Bradford, M. and Azhari, M. (1995), "Buckling of plates with different end conditions using the finite strip method", *Comput. Struct.*, **56**(1), 75-83.

Davies, J.M., Leach, P. and Heinz, D. (1994), "Second-order generalised beam theory", *J. Constructional Steel Research*, **31**(2-3), 221-241.

Davies, J.M. and Jiang, C. (1998), "Design for distortional buckling", *J. Constructional Steel Research*, **46**(1-3), 174. (CD-ROM paper #104)

Hancock, G.J. (1985), "Distortional buckling of steel storage rack columns", *J. Struct. Eng.* (ASCE), **111**(12), 2770-2783.

Hancock, G.J. (1997), "Design for distortional buckling of flexural members", *Thin-Walled Structures*, **27**(1), 3-12.

Lau, S. and Hancock, G.J. (1987), "Distortional buckling formulae for channel columns", *J. Struct. Eng.* (ASCE), **113**(5), 1063-1078.

Lau, S. (1988), "Distortional buckling of thin-walled columns", Ph.D. Thesis, School of Civil and Mining Engineering, University of Sydney.

Schafer, B. (1997), "Cold-formed steel behavior and design: analytical and numerical modelling of elements and members with longitudinal stiffeners", Ph.D. Thesis, Cornell University.

Schardt, R. (1989), *Verallgemeinerte Technische Biegetheorie*, Springer Verlag, Berlin. (German)

Schardt, R. (1994a), "Generalized beam theory - an adequate method for coupled stability problems", *Thin-Walled Structures*, **19**(2-4), 161-180.

Schardt, R. (1994b), "Lateral torsional and distortional buckling of channel and hat-sections", *J. Constructional Steel Research*, **31**(2-3), 243-265.

Silvestre, N., Nagahama, K., Camotim, D. and Batista, E. (2002), "GBT-based distortional buckling formulae for thin-walled rack-section columns and beams", *Advances in Steel Structures (ICASS'02)*, Chan, S.L., Teng, J.G. and Chung, K.F. (eds.), Elsevier, Hong Kong, December 9-11, 341-350 (vol. 1).

Silvestre, N. and Camotim, D. (2002a), "First order generalised beam theory for arbitrary orthotropic materials", *Thin-Walled Structures*, **40**(9), 755-789.

Silvestre, N. and Camotim, D. (2002b), "Second order generalised beam theory for arbitrary orthotropic materials", *Thin-Walled Structures*, **40**(9), 791-820.

Silvestre, N. and Camotim, D. (2003). "Distortional buckling formulae for cold-formed steel C and Z-section members", submitted for publication.

Standards Association of Australia (1996), *The Australian/New Zealand Cold-Formed Steel Structures Standard*, AS/NZS 4600.

Teng, J.G., Yao, J. and Zhao, Y. (2003), "Distortional buckling of channel beam-columns", *Thin-Walled Structures*, **41**(7), 595-617.

Van der Maas, C.J. (1954), "Charts for the calculation of the critical compressive stress for local instability of

columns with hat sections", *J. the Aeronautical Sciences*, **21**(6), 399-403.
Waterloo Maple Software (2001). MAPLE V (release 7), University of Waterloo, Canada.

Annex - Analytical definition of the auxiliary eigenvalue problem

To define the auxiliary eigenvalue problem (Eq. 27), one needs expressions for the *non-null* components of matrices **F**, $\ddot{\mathbf{w}}$ and **C**. Noticing that **F** and **C** are *symmetric*, one has:

$$F_{11} = F_{22} = F_{77} = F_{88} = 1 \qquad F_{33} = F_{66} = \frac{1}{3K} b_w(\alpha_f + \alpha_s)$$

$$F_{44} = F_{55} = \frac{1}{3K} b_w(\alpha_f + 1) \qquad F_{34} = F_{56} = \frac{1}{6K} b_w \alpha_f \qquad F_{45} = \frac{1}{6K} b_w$$

$$C_{11} = C_{88} = 2C_{12} = 2C_{78} = \frac{1}{3}\alpha_l b_w t \quad C_{22} = C_{77} = \frac{1}{3}(\alpha_s + \alpha_l) b_w t \quad C_{23} = C_{67} = \frac{1}{6}\alpha_s b_w t$$

$$C_{33} = C_{66} = \frac{1}{3}(\alpha_f + \alpha_s) b_w t \quad C_{44} = C_{55} = \frac{1}{3}(\alpha_f + 1) b_w t \quad C_{34} = C_{56} = \frac{1}{6}\alpha_f b_w t \quad C_{45} = \frac{1}{6} b_w t$$

$$\ddot{w}_{31} = \ddot{w}_{68} = \frac{1}{\alpha_l \alpha_s b_w^2 \sin\theta} \quad \ddot{w}_{32} = \ddot{w}_{67} = \frac{1}{\alpha_s b_w^2 \sin\theta}\left(\frac{1}{\alpha_f} - \frac{1}{\alpha_l}\right) \quad \ddot{w}_{42} = \ddot{w}_{57} = -\frac{1}{\alpha_f \alpha_s b_w^2 \sin\theta}$$

$$\ddot{w}_{33} = \ddot{w}_{66} = -\frac{1}{\alpha_f b_w^2}\left(\frac{1}{\alpha_f \tan\theta} + \frac{2}{\alpha_s \sin\theta}\right) \quad \ddot{w}_{34} = \ddot{w}_{65} = \ddot{w}_{43} = \ddot{w}_{56} = \frac{1}{\alpha_f b_w^2}\left(1 + \frac{1}{\alpha_f \tan\theta} + \frac{1}{\alpha_s \sin\theta}\right)$$

$$\ddot{w}_{35} = \ddot{w}_{64} = \ddot{w}_{46} = \ddot{w}_{53} = -\frac{1}{\alpha_f b_w^2} \quad \ddot{w}_{45} = \ddot{w}_{54} = \frac{2}{\alpha_f b_w^2} \quad \ddot{w}_{44} = \ddot{w}_{55} = -\frac{1}{\alpha_f b_w^2}\left(2 + \frac{1}{\alpha_f \tan\theta}\right)$$

CC